

Journal of Biomedical Optics

BiomedicalOptics.SPIEDigitalLibrary.org

Noninvasive photoacoustic microscopy of methemoglobin *in vivo*

Min Tang
Yong Zhou
Ruiying Zhang
Lihong V. Wang

SPIE.

Noninvasive photoacoustic microscopy of methemoglobin *in vivo*

Min Tang,[†] Yong Zhou,[†] Ruiying Zhang, and Lihong V. Wang^{*}

Washington University in St. Louis, Department of Biomedical Engineering, Optical Imaging Laboratory, One Brookings Drive, St. Louis, Missouri 63130, United States

Abstract. Due to the various causes of methemoglobinemia and its potential to be confused with other diseases, *in vivo* measurements of methemoglobin have significant applications in the clinic. Using photoacoustic microscopy (PAM), we quantified the average and the distributed percentage of methemoglobin both *in vitro* and *in vivo*. Based on the absorption spectra of methemoglobin, oxyhemoglobin, and deoxyhemoglobin, three wavelengths were chosen to differentiate methemoglobin from the others. The methemoglobin concentrations calculated from the photoacoustic signals agreed well with the preset concentrations. Then we imaged the methemoglobin percentage in microtubes that mimicked blood vessels. Average percentages calculated for five samples with different methemoglobin concentrations also agreed well with the preset values. Finally, we demonstrated the ability of PAM to detect methemoglobin *in vivo* in a mouse ear. Our results show that PAM can quantitatively image methemoglobin distribution *in vivo*. © 2015 Society of Photo-Optical Instrumentation Engineers (SPIE) [DOI: 10.1117/1.JBO.20.3.036007]

Keywords: photoacoustic microscopy; methemoglobin; distributed percentage *in vivo*.

Paper 140818R received Dec. 9, 2014; accepted for publication Feb. 20, 2015; published online Mar. 11, 2015.

1 Introduction

Methemoglobin is an abnormal type of hemoglobin that contains oxidized iron atoms in the ferric state and is incapable of transporting oxygen to body tissues.^{1,2} Elevated methemoglobin levels (methemoglobinemia) can cause tachycardia, stupor, and impaired respiration due to tissue hypoxia. Death may occur in humans when the methemoglobin level in the blood stream is >70%.³ More common than the congenital form, acquired methemoglobinemia may be induced by a wide range of chemicals and drugs. Local anesthetics, such as topical benzocaine, antibiotics such as dapson, and nitrites in well water or additives to preserve meat, can all lead to methemoglobinemia.⁴⁻⁶ Thus, measuring the methemoglobin level has extensive clinical applications. In addition to measuring the average concentration, measuring the spatial distribution of methemoglobin provides important information for the diagnosis and treatment of diseases. Methemoglobinemia secondary to topical anesthetics has been reported in many clinical contexts and is potentially lethal.^{7,8} Usually used as a treatment for methemoglobinemia, methylene blue can worsen the condition in individuals with endogenous glucose-6-phosphate dehydrogenase deficiency.^{9,10} In this case, fast measurement of the spatial distribution of methemoglobin around the area where anesthetics are applied enables surgeons to react quickly by revealing the concentration change of methemoglobin following the treatment. Moreover, measuring methemoglobin's spatial distribution provides additional information for differential diagnoses in patients with mechanical airway obstruction, pulmonary embolus, or circulatory shock,⁴ and in infants with cyanotic congenital heart diseases or sepsis.⁵ Finally, spatial distribution measurements

can potentially provide opportunities to study the role of methemoglobin in inflammation and atherosclerotic diseases.⁹

Current techniques for methemoglobin detection, including arterial blood gas analysis, pulse oximetry, and co-oximetry, are limited in various ways. Arterial blood gas analysis will show a normal partial pressure of oxygen even when the methemoglobin concentration is high because it measures only the dissolved oxygen, not the actual amount of oxygen bound to hemoglobin in blood.^{5,11} Pulse oximetry measures arterial blood oxygenation using two light sources of different wavelengths (typically 660 and 940 nm), which works well when only oxyhemoglobin and deoxyhemoglobin are present. However, methemoglobin absorbs light equally well at these two wavelengths, which drives the value of red-to-infrared ratio to one.^{12,13} Based on the algorithm of pulse oximetry, a ratio of one corresponds to an oxygen saturation of 85%,^{11,13} which is an unreliable result at high levels of methemoglobin. In addition, at 660 nm, methemoglobin has a molar absorption coefficient similar to that of deoxyhemoglobin, which could also confound the measurement.¹¹ Co-oximetry is a generally accurate method for measurement of methemoglobin, but the readings can also be falsely positive in the presence of methylene blue, which is commonly used for treatment.^{11,14} Furthermore, all of these conventional diagnostic modalities measure only the average concentration, not the spatial distribution, of methemoglobin. We still lack a technique that can spatially image the concentrations of methemoglobin quantitatively *in vivo*.

Since it was first introduced in 2005, three-dimensional photoacoustic microscopy (PAM) has demonstrated its potential in structural and functional imaging.¹⁵⁻²⁰ In PAM, a short-pulsed laser is used to irradiate the object. When the light is absorbed by the object, the resulting temperature rise leads to an initial

*Address all correspondence to: Lihong V. Wang, E-mail: lhwang@wustl.edu

[†]The authors contributed equally to this work.

pressure rise in proportion to the local energy deposition. The initial pressure rise then propagates as photoacoustic waves which can be detected by a focused ultrasonic transducer.²¹ Excitation at multiple optical wavelengths in PAM can provide spectral information concerning the optical absorption.²² So far, PAM has successfully detected a number of endogenous optical absorbers *in vivo*, such as oxyhemoglobin, deoxyhemoglobin, carboxyhemoglobin, bilirubin, and melanin.^{23–25}

The motivation of this work is to quantitatively image methemoglobin distribution with PAM. We first demonstrated that our PAM system was able to differentiate methemoglobin from oxyhemoglobin and deoxyhemoglobin in bovine blood. A 3.1% root mean square error of prediction (RMSEP), which defines the accuracy of the measurement, was achieved for the measurements of methemoglobin *in vitro*. In addition, methemoglobin distributions were successfully detected in vessel-mimicking phantoms. Finally, the methemoglobin distribution in a mouse ear was imaged *in vivo* during a period of induction and recovery of methemoglobin. We showed for the first time that PAM can quantitatively image the spatial distribution of methemoglobin both *in vitro* and *in vivo*.

2 Material and Methods

2.1 Experimental System

An optical-resolution PAM system^{26,27} was used to measure methemoglobin distribution, as shown in Fig. 1. The light source was a tunable dye laser (CBR-D, Sirah GmbH) pumped by an Nd:YLF laser (INNOSAB, Edgewave GmbH) at a 1 kHz pulse repetition rate with pulse width around 5 ns. 4-dicyanomethylene-2-methyl-6-p-dimethylaminostyryl-4H-pyran dissolved in ethanol was used to generate a laser beam with a wavelength tunable from 595 to 665 nm. The laser beam was focused by a lens, filtered by a pinhole, and reflected by a mirror toward an objective lens to be focused into the object. An acoustic-optical beam combiner containing two prisms with a layer of silicone oil in between provided the acoustic optical coaxial alignment. Then a wideband ultrasonic transducer (V214-BC, Panametrics-NDT Inc.) with a center frequency around 50 MHz (70% two-way bandwidth) detected the acoustic signals. A spherically focused acoustic lens, with a focal distance

around 6 mm, was placed confocally with the optical objective lens. A depth-resolved one-dimensional (1-D) photoacoustic A-line signal was obtained from each laser pulse. The Hilbert transformation was applied to the 1-D photoacoustic signals for envelope extraction. By raster scanning the object in two dimensions and performing maximum amplitude projections (MAP) of the A-line signals, a two-dimensional MAP PAM image of the sample was obtained.

2.2 Phantom Preparations

Sodium nitrite (237213-500G, Sigma-Aldrich) powder was mixed with lysed bovine blood (905, Quad-Five) to induce methemoglobin formation in the samples. To induce a level of 100% methemoglobin, 24.3 g sodium nitrite powder was added to 50 ml of bovine blood. Then blood samples with methemoglobin concentrations of 20, 40, 60, and 80% were obtained by mixing 2, 4, 6, and 8 ml of the 100% methemoglobin blood with 8, 6, 4, and 2 ml of pure bovine blood, respectively. The mixtures were then separately injected into microtubes (60985-700, VWR) made of platinum-cured silicone, with 300 μm inner diameters and 600 μm outer diameters, to mimic blood with different methemoglobin concentrations in blood vessels.

2.3 In Vivo Methemoglobin Induction in a Mouse Model

To induce methemoglobin formation in a mouse model, 60 μl of the well-mixed sodium nitrite solution (10 mg sodium nitrite/1 ml de-ionized water) was injected through the jugular vein of a mouse. The volume and concentration were calculated based on the Kohn's model.²⁸ Subsequently, the blood vessels of the mouse ear were imaged by the PAM system at multiple optical wavelengths.

2.4 Quantification of Methemoglobin, Oxyhemoglobin, and Deoxyhemoglobin Concentrations

The absorbance (A) of the sample measured by a spectrophotometer can be expressed as

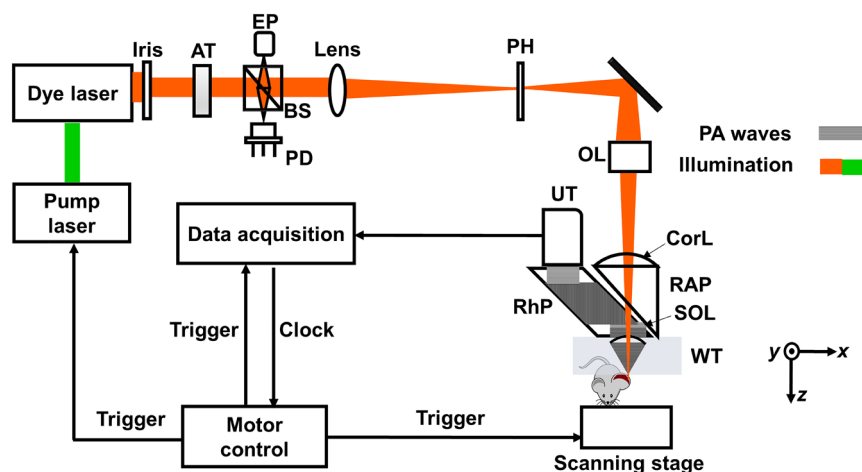


Fig. 1 Schematic of photoacoustic microscopy (PAM) system. AT, attenuator; BS, beam splitter; CorL, correction lens; EP, eyepiece; OL, objective lens; PD, photodiode; PH, pinhole; RAP, right-angle prism; RhP, rhomboid prism; SOL, silicone oil layer; UT, ultrasonic transducer; WT, water tank.

$$A = \ln 10 \times [c_{\text{oxy}}\epsilon_{\text{oxy}}(\lambda) + c_{\text{deoxy}}\epsilon_{\text{deoxy}}(\lambda) + c_{\text{met}}\epsilon_{\text{met}}(\lambda)], \quad (1)$$

where c_{oxy} , c_{deoxy} , and c_{met} are the concentrations of oxyhemoglobin, deoxyhemoglobin, and methemoglobin, respectively; $\epsilon_{\text{oxy}}(\lambda)$, $\epsilon_{\text{deoxy}}(\lambda)$, and $\epsilon_{\text{met}}(\lambda)$ are the wavelength-dependent molar absorption coefficients of oxyhemoglobin, deoxyhemoglobin, and methemoglobin, respectively. In theory, three wavelengths are enough to calculate the concentrations of all three forms of hemoglobin. The methemoglobin percentage can be calculated by $c_{\text{met}}/C_{\text{Hb}}$, where C_{Hb} is the total hemoglobin concentration.

The photoacoustic amplitude $[\varphi(\lambda)]$ can be described as

$$\varphi(\lambda) = k[c_{\text{oxy}}\epsilon_{\text{oxy}}(\lambda) + c_{\text{deoxy}}\epsilon_{\text{deoxy}}(\lambda) + c_{\text{met}}\epsilon_{\text{met}}(\lambda)], \quad (2)$$

where k is a sample-independent constant factor, including the Grueneisen parameter, heat conversion percentage, and other minor contributors.²⁹ Similar to how the methemoglobin percentage is calculated with the spectrophotometric measurements, the methemoglobin percentage can be calculated with photoacoustic measurements acquired at three wavelengths.

Given both the systematic and random errors, we can define the measurement accuracy by RMSEP.²³

$$\text{RMSEP} = \sqrt{e_s^2 + e_r^2}, \quad (3)$$

where e_s represents the systematic error and e_r represents the random error:

$$e_s = \sqrt{\frac{\sum_{i=1}^n (M_i - C_i)^2}{n}}, \quad (4)$$

$$e_r = \sqrt{\frac{\sum_{i=1}^n \delta M_i^2}{n}}, \quad (5)$$

where C_i , M_i , and δM_i are the preset concentration, average measured concentration, and the standard deviation of the i 'th sample, respectively, and n is the total number of samples.

3 Results

3.1 Photoacoustic Spectra and Measurement Accuracy

As shown by the molar extinction spectra^{30,31} in Fig. 2(a), methemoglobin has stronger absorption than oxyhemoglobin and deoxyhemoglobin, from 610 to 630 nm. Four phantoms with different methemoglobin concentrations (20, 40, 60, and 80%) were first measured by a spectrophotometer (Cary 50 Bio UV/Visible, VARIAN). The measured absorption coefficient shows an increasing trend in the chosen range (610 to 630 nm) as the methemoglobin level increases [Fig. 2(b)]. Then the four samples were measured by the PAM system. As expected, the intensity of the photoacoustic signals increased from the 20% methemoglobin to the 80% methemoglobin [Fig. 2(c)]. The trends of the photoacoustic signals from 610 to 630 nm for each concentration also agree with the results from the spectrophotometer. Additionally, the percentage of methemoglobin and oxyhemoglobin measured by the PAM system all fit the preset concentrations well [Fig. 2(d)]. The 3.1%

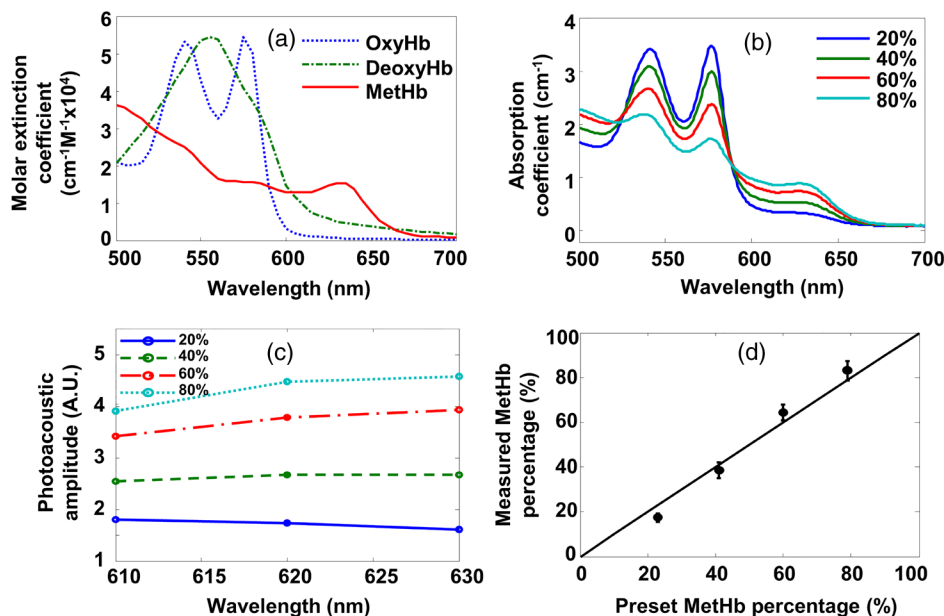


Fig. 2 (a) Molar extinction coefficients of oxyhemoglobin (OxyHb), deoxyhemoglobin (DeoxyHb), and methemoglobin (MetHb) versus optical wavelength. (b) Absorption coefficient of blood samples that are further diluted 20 times measured with spectrophotometry. 20, 40, 60, and 80% refer to the methemoglobin percentage of the total hemoglobin. (c) Photoacoustic signals of blood samples measured at three optical wavelengths: 610, 620, and 630 nm. (d) Methemoglobin percentage of each sample measured using PAM versus the preset value. Circles: photoacoustically measured methemoglobin percentages. Line: ideal fit if the photoacoustically measured and preset methemoglobin percentages were identical.

RMSEP of the concentration also validated that our *in vitro* measurements were relatively accurate.

3.2 Quantitative Methemoglobin Imaging in Phantoms

Methemoglobin distributions were imaged by PAM in tissue-mimicking phantoms. Samples with different induced methemoglobin levels were prepared with the method described above. Five microtubes filled with bovine blood having average methemoglobin concentrations of 23, 41, 58, 76, and 89% were used to mimic blood vessels with blood of different methemoglobin levels. The same wavelengths were selected for PAM imaging, with a scanning area of 4 mm by 2 mm. The normalized PAM images obtained at each wavelength are shown in Fig. 3(a). The methemoglobin distribution is calculated for each pixel in the coregistered multiwavelength images. To reduce the impact of noise, we only analyzed those pixels with signal-to-noise ratio higher than five. Based on these multiwavelength images, the calculated distributions of methemoglobin concentrations are shown in Fig. 3(b). We showed that the PAM results averaged within each tube accorded well with the preset concentrations, as shown in Fig. 3(c). The results in Fig. 3 demonstrate that PAM is capable of imaging the concentration and distribution of methemoglobin in blood.

3.3 Methemoglobin Imaging In Vivo in a Mouse Ear

Finally, to demonstrate PAM imaging of methemoglobin *in vivo*, methemoglobin formation was induced in a mouse with sodium nitrite solution.²⁸ The mouse ear was imaged by PAM

consecutively for ~105 min to include both the methemoglobin-induction activity and the recovery activity of the mouse's self-reductive systems. An area of 4 mm by 4 mm was first scanned to show the blood vessels on the mouse's ear [Fig. 4(a)] with a wavelength of 610 nm; then a 1 mm by 0.6 mm area was imaged at the three wavelengths (610, 620, and 630 nm) once every 4 min, to monitor the change in methemoglobin level over the 105 min [the rectangular area in Fig. 4(a)]. As shown in Fig. 4(b1), methemoglobin percentage was low in the blood before the injection of sodium nitrite solution. We observed an increase of methemoglobin percentage due to the injection of sodium nitrite solution [Fig. 4(b2)] followed by a decrease of the methemoglobin percentage due to the self-reductive mechanism [Figs. 4(b3) and 4(b4)]. The time course of the average methemoglobin and oxyhemoglobin percentages measured by PAM [Fig. 4(c)] were in accordance with the prediction of the Kohn model.²⁸

4 Discussions and Conclusions

Within the chosen range of wavelengths in this work (from 610 to 630 nm), the absorption in blood vessels mainly originates from oxyhemoglobin, deoxyhemoglobin, and methemoglobin. For the three absorbers in this experiment, three optical wavelengths are enough to differentiate methemoglobin from oxyhemoglobin and deoxyhemoglobin. While using more wavelengths can provide additional data for a more accurate least squares fit, the measurement would take longer. The choice between accuracy and speed depends on the application of the technique.

In healthy humans, the level of methemoglobin is very low, so the oxyhemoglobin and deoxyhemoglobin absorb most of the

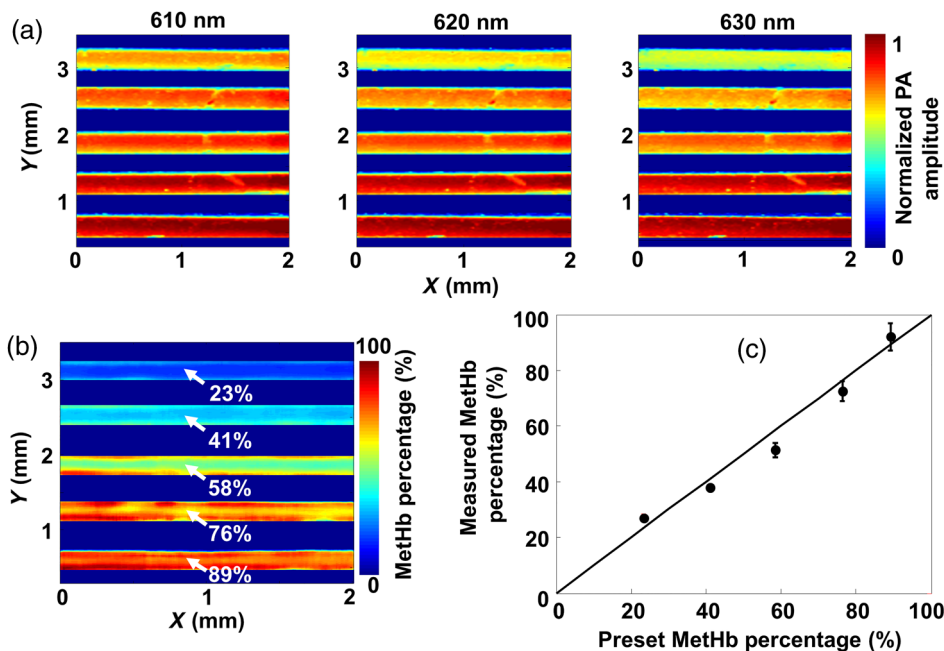


Fig. 3 (a) Maximum-amplitude projection (MAP) PAM images of tubes filled with different concentrations of methemoglobin in lysed bovine blood at 610, 620, and 630 nm. (b) Methemoglobin distribution image calculated from the multiwavelength PAM images. The average methemoglobin percentages from top to bottom are 23, 41, 58, 76, and 89%. (c) The photoacoustically measured methemoglobin and oxyhemoglobin percentage averaged within each tube versus the preset value. The preset percentages were measured with a spectrophotometer. Circles: photoacoustically versus spectrophotometrically measured methemoglobin percentages. Line: ideal fit if the photoacoustically measured and preset methemoglobin percentages were identical. Data are presented as the mean \pm standard error (based on four measurements).

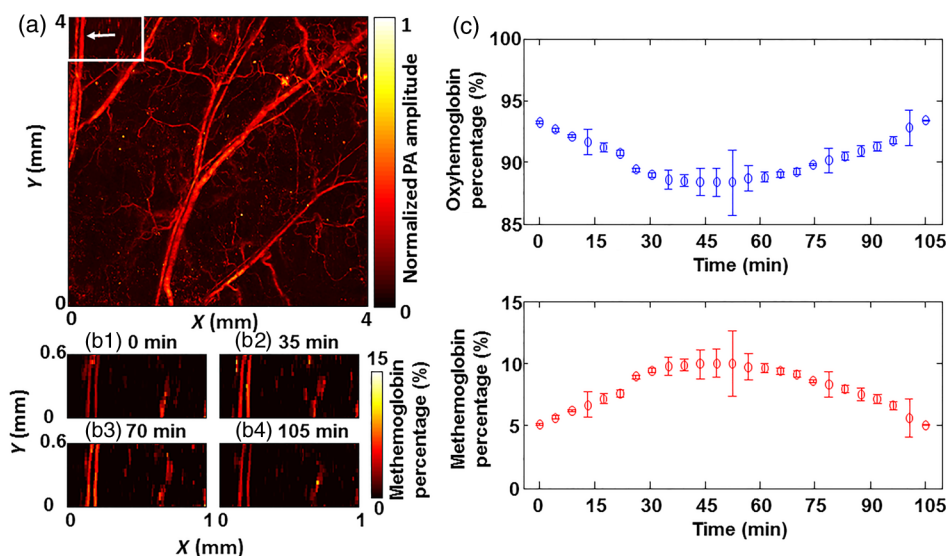


Fig. 4 (a) MAP PAM image of blood vessels of a mouse ear acquired at a wavelength of 610 nm. The vessel indicated by the arrow in the white rectangle was monitored to calculate the methemoglobin level during the induction and self-recovery periods. (b1–b4) Spatial distribution of methemoglobin percentages measured every 35 min after the intravenous injection of sodium nitrite solution. (c) Time course of methemoglobin and oxyhemoglobin average percentages before and after intravenous injection of sodium nitrite solution. Data are presented as the mean \pm standard error (based on four measurements).

optical energy. In this case, PAM alone may not be able to provide accurate absolute quantification. However, it can complement other traditional measuring techniques to image the spatial distribution of methemoglobin.

To the best of our knowledge, this is the first study to use PAM to quantitatively image the methemoglobin *in vivo*. The methemoglobin concentration and distribution were imaged by PAM in tissue-mimicking phantoms at multiple wavelengths. In the phantom study, the RMSEP of the concentration was calculated to be 3.1%. We also measured the methemoglobin concentration change *in vivo* after induction of methemoglobinemia in a mouse. After intravenous injection of sodium nitrite solution, the methemoglobin level measured in the blood vessels of the mouse ear increased from 5 to 10% and peaked \sim 45 min after injection. The methemoglobin concentration gradually decreased to the normal level by the end of the measurement. This finding is in accordance with the prediction of the Kohn model.²⁸ Our study demonstrated PAM's capability to quantify methemoglobin levels *in vivo*, with potential clinical applications.

Acknowledgments

The authors gratefully acknowledge the suggestions made by the reviewers of this manuscript, by Professor James Ballard and by Professor Sandra Matteucci at Washington University in St. Louis. This work was supported in part by National Institutes of Health grants DP1 EB016986, R01 CA186567, U01 NS090579, R01 EB016963, R01 EB010049, R01 CA157277, S10 RR028864, S10 RR026922, and R01 CA159959 as well as National Science Foundation grant 1255930. L.V.W. has a financial interest in Microphotoacoustics Inc., and Endra Inc., which, however, did not support this work.

References

1. N. E. Camp, "Methemoglobinemia," *J. Emerg. Nurs.* **33**(2), 172–174 (2007).
2. S. Bradberry, "Methaemoglobinaemia," *Medicine* **40**(2), 59–60 (2012).

3. H. U. Rehman, "Methemoglobinemia," *West. J. Med.* **175**(3), 193–196 (2001).
4. J. A. Cortazzo and A. D. Lichtman, "Methemoglobinemia: a review and recommendations for management," *J. Cardiothorac. Vasc. Anesth.* **28**(4), 1055–1059 (2014).
5. R. O. Wright, W. J. Lewander, and A. D. Woolf, "Methemoglobinemia: etiology, pharmacology, and clinical management," *Ann. Emerg. Med.* **34**(5), 646–656 (1999).
6. J. N. Lukens, "Landmark perspective: the legacy of well-water methemoglobinemia," *JAMA* **257**(20), 2793–2795 (1987).
7. D. R. Lorelli, D. E. Morris, and J. W. Lewis Jr., "Drug-induced methemoglobinemia during thoroscopic lung biopsy," *Ann. Thorac. Surg.* **71**(2), 703–705 (2001).
8. R. Gutta and P. J. Louis, "Methemoglobinemia—an unusual cause of intraoperative hypoxia," *Oral Surg. Oral Med. Oral Pathol. Oral Radiol. Endod.* **103**(2), 197–202 (2007).
9. J. Umbreit, "Methemoglobin—it's not just blue: a concise review," *Am. J. Hematol.* **82**(2), 134–144 (2007).
10. S. Patnaik et al., "Methylene blue unresponsive methemoglobinemia," *Indian J. Crit. Care Med.* **18**(4), 253–255 (2014).
11. E. D. Chan, M. M. Chan, and M. M. Chan, "Pulse oximetry: understanding its basic principles facilitates appreciation of its limitations," *Respir. Med.* **107**(6), 789–799 (2013).
12. A. Jubran, "Pulse oximetry," *Crit. Care* **3**(2), R11–R17 (1999).
13. L. M. Schnapp and N. H. Cohen, "Pulse oximetry. Uses and abuses," *Chest* **98**(5), 1244–1250 (1990).
14. J. Lee et al., "Noninvasive *in vivo* monitoring of methemoglobin formation and reduction with broadband diffuse optical spectroscopy," *J. Appl. Physiol.* **100**(2), 615–622 (2006).
15. K. Maslov, G. Stoica, and L. V. Wang, "In vivo dark-field reflection-mode photoacoustic microscopy," *Opt. Lett.* **30**(6), 625–627 (2005).
16. H. F. Zhang et al., "Functional photoacoustic microscopy for high-resolution and noninvasive *in vivo* imaging," *Nat. Biotechnol.* **24**(7), 848–851 (2006).
17. K. Maslov et al., "Optical-resolution photoacoustic microscopy for *in vivo* imaging of single capillaries," *Opt. Lett.* **33**(9), 929–931 (2008).
18. L. V. Wang, "Multiscale photoacoustic microscopy and computed tomography," *Nat. Photonics* **3**(9), 503–509 (2009).
19. S. Hu and L. V. Wang, "Photoacoustic imaging and characterization of the microvasculature," *J. Biomed. Opt.* **15**(1), 011101 (2010).
20. L. V. Wang and S. Hu, "Photoacoustic tomography: *in vivo* imaging from organelles to organs," *Science* **335**(6075), 1458–1462 (2012).

21. L. V. Wang and H. Wu, *Biomedical Optics: Principles and Imaging*, 1st ed., Wiley, Hoboken, NJ (2007).
22. J. Yao et al., "Label-free oxygen-metabolic photoacoustic microscopy *in vivo*," *J. Biomed. Opt.* **16**(7), 076003 (2011).
23. Y. Zhou et al., "Photoacoustic microscopy of bilirubin in tissue phantoms," *J. Biomed. Opt.* **17**(12), 126019 (2012).
24. Y. Zhou et al., "Handheld photoacoustic microscopy to detect melanoma depth *in vivo*," *Opt. Lett.* **39**(16), 4731–4734 (2014).
25. Z. Chen, S. Yang, and D. Xing, "*In vivo* detection of hemoglobin oxygen saturation and carboxyhemoglobin saturation with multiwavelength photoacoustic microscopy," *Opt. Lett.* **37**(16), 3414–3416 (2012).
26. P. Hai et al., "Near-infrared optical-resolution photoacoustic microscopy," *Opt. Lett.* **39**(17), 5192–5195 (2014).
27. Y. Zhou, J. Yao, and L. V. Wang, "Optical clearing-aided photoacoustic microscopy with enhanced resolution and imaging depth," *Opt. Lett.* **38**(14), 2592–2595 (2013).
28. M. C. Kohn et al., "Pharmacokinetics of sodium nitrite-induced methemoglobinemia in the rat," *Drug Metab. Dispos.* **30**(6), 676–683 (2002).
29. Y. Zhou et al., "Calibration-free absolute quantification of particle concentration by statistical analyses of photoacoustic signals *in vivo*," *J. Biomed. Opt.* **19**(3), 037001 (2014).
30. L. L. Randeberg et al., "Methemoglobin formation during laser induced photothermolysis of vascular skin lesions," *Lasers Surg. Med.* **34**(5), 414–419 (2004).
31. S. Prahl, "Optical absorption of hemoglobin," 1999, <http://omlc.org/spectra/hemoglobin/>.

Min Tang is currently a senior undergraduate student in the Department of Biomedical Engineering at Washington University in St. Louis. Her research interests include tissue engineering and its related applications.

Yong Zhou is currently a graduate student in biomedical engineering at Washington University in St. Louis, under the supervision of Dr. Lihong V. Wang, Gene K. Beare distinguished professor. His research focuses on the development of photoacoustic imaging systems.

Ruiying Zhang received her BS in optical information science and technology from Wuhan University in Hubei, China. She is currently a PhD student in the Department of Biomedical Engineering at Washington University in St. Louis. Her research interests include optical and photoacoustic imaging with biomedical applications.

Lihong Wang, the Beare distinguished professor at Washington University, has published 420 journal articles (h-index=93, citations > 35,000) and delivered 400 keynote/plenary/invited talks. His laboratory published the first functional photoacoustic CT and three-dimensional photoacoustic microscopy. He received the Goodman Award for his *Biomedical Optics* textbook, NIH Director's Pioneer Award, OSA Mees Medal, IEEE Technical Achievement and Biomedical Engineering Awards, SPIE Britton Chance Biomedical Optics Award, and an honorary doctorate from Lund University, Sweden.